PCCP

PAPER

View Article Online
View Journal | View Issue

Cite this: *Phys. Chem. Chem. Phys.*, 2017, **19**, 8471

Prediction of thermodynamically stable Li–B compounds at ambient pressure†

Dian-Hui Wang,[a] Huai-Ying Zhou,[abc] Chao-Hao Hu,*[bc] Yan Zhong,[bcd] Artem R. Oganov[efg] and Guang-Hui Rao[bc]

Received 30th December 2016,
Accepted 23rd February 2017

DOI: 10.1039/c6cp08900c

rsc.li/pccp

To clarify controversial structures and phase stability in the Li–B system, we predicted energetically favorable compounds and crystal structures of the Li–B binary system at ambient pressure, mainly including Li_6B_5, LiB_2, and LiB_3, from *ab initio* evolutionary structure simulations and further investigated physical properties of stable Li–B compounds using first-principles methods. Metallic Li_6B_5, predicted in our simulations, has trigonal symmetry with space group *R*32 and contains linear B chains, but its superconducting T_c is low according to the electron–phonon coupling calculations. Orthorhombic LiB_2 (*Pnma*) and tetragonal LiB_3 (*P*4/*mbm*) are zero-gap semiconductors; LiB_2 is a Dirac semimetal, and both LiB_2 and LiB_3 are promising thermoelectric materials.

Introduction

Atoms of light elements have simple electronic structures, but can form complex compounds possessing extraordinary properties. Boron is electron-deficient and boron-based compounds being likely to form multicenter bonds[1,2] are often accompanied by complicated crystal structures and stoichiometries. After the discovery of high-T_c superconductivity in MgB_2,[3] borides of light metals have attracted much attention. Compounds of the lightest metal lithium with the lightest solid nonmetal boron can have many interesting properties, warranting an investigation.

Many investigations have been carried out to explore possible compositions in the Li–B system, but only a few compounds are well characterized. Nesper *et al.* have confirmed tetragonal Li_3B_{14} ($I\bar{4}2d$)[4] and successfully prepared dark red transparent crystals of LiB_3 (*P*4/*mbm*).[5] Lithium borides close to the stoichiometric ratio 1 : 1 have been intensively studied. Wang *et al.* reported the preparation of LiB and claimed that the compound is Li_5B_4 with a rhombohedral crystal structure.[6,7] Similar stoichiometries, *e.g.*, Li_6B_7 and $Li_{1.06}B$,[8,9] were reported later. Liu *et al.* experimentally studied LiB[10] by X-ray diffraction and found that the stoichiometric LiB has hexagonal symmetry with space group $P6_3/mmc$. Theoretical results from Rosner *et al.*[11] showed that the electron–phonon coupling effect in hexagonal LiB is rather small. Recently, based on the X-ray and neutron powder diffraction data, Wörle and Nesper concluded that LiB_x ($0.82 < x \leq 1.0$) has an extraordinary crystal structure which contains linear carbyne-like boron chains with strong covalent bonds between boron atoms.[12] However, more detailed structural information on this compound is still absent and the corresponding physical properties need to be studied systematically. Here we present a theoretical study of the Li–B system, clarifying stable compositions, crystal structures and physical properties of lithium borides by first-principles methods.

Computational details

The *ab initio* evolutionary structure prediction method as implemented in the USPEX (Universal Structure Predictor: Evolutionary Xtallography) code[13,14] was employed to determine the energetically favorable compositions and structures in the Li–B system at ambient pressure. USPEX has been widely used to predict the lowest-enthalpy structures without any experimental data.[13–16] Especially, besides the traditional fixed-composition search (FCS), the recently developed variable-composition search (VCS) in the USPEX code[17,18] allows one to predict stable stoichiometries. Structure relaxations and total energy calculations were performed

[a] *School of Materials Science and Engineering, Central South University, Changsha 410083, P. R. China*
[b] *Guangxi Key Laboratory of Information Materials, Guilin University of Electronic Technology, Guilin 541004, P. R. China. E-mail: chaohao.hu@guet.edu.cn*
[c] *School of Materials Science and Engineering, Guilin University of Electronic Technology, Guilin 541004, P. R. China*
[d] *Guangxi Experiment Center of Information Science, Guilin University of Electronic Technology, Guilin 541004, P. R. China*
[e] *Skolkovo Institute of Science and Technology, Skolkovo Innovation Center, 3 Nobel St., Moscow 143026, Russia*
[f] *Moscow Institute of Physics and Technology, 9 Institutskiy Lane, Dolgoprudny City, Moscow Region 141700, Russia*
[g] *Department of Geosciences and Center for Materials by Design, State University of New York, Stony Brook, NY 11794-2100, USA*

† Electronic supplementary information (ESI) available: Optimized structural parameters of other metastable Li–B compounds like Li_6B_5, Li_5B_4, Li_7B_6, LiB_4, and LiB_6 at ambient pressure. See DOI: 10.1039/c6cp08900c

within density functional theory as implemented in the Vienna *Ab Initio* Simulation Package (VASP).[19] The projector augmented wave (PAW) method[20] was used to describe the interaction between electrons and cores, and the generalized gradient approximation functional of Perdew, Burke and Ernzerhof[21] was used to treat the exchange–correlation energy. In the PAW potentials, electronic configurations $1s^2 2s^1$ and $2s^2 2p^1$ were treated as valence for Li and B, respectively. A cutoff energy of 540 eV for plane wave basis sets and dense Γ-centered k-point meshes with a reciprocal-space resolution of $2\pi \times 0.03$ Å^{-1} were used for all the structures to ensure sufficient convergence of the energy, forces and stress tensor. For the predicted stable crystal structures, the GW approximation[22] was used for obtaining more accurate electronic structures.

Lattice dynamics were calculated using the frozen phonon method as implemented in the Phonopy package.[23] Force constant matrices were determined using the $2 \times 2 \times 2$, $2 \times 2 \times 2$, and $2 \times 2 \times 3$ supercells for Li_6B_5, LiB_2 and LiB_3, respectively. In addition, to investigate the possibility of superconducting state in Li_6B_5, electron–phonon coupling (EPC) calculations were carried out using density-functional perturbation theory, as implemented in the Quantum Espresso (QE) package.[24] For self-consistent calculations in QE, Vanderbilt-type ultrasoft pseudopotentials with a kinetic cutoff energy of 180 Ry for wave functions and a $16 \times 16 \times 16$ MP k-point grid with a Gaussian smearing of 0.05 Ry were used, together with a $6 \times 6 \times 6$ q-mesh, which ensures that the electron–phonon matrix elements are well converged.

Thermoelectric properties of Li–B compounds were calculated using Boltztrap,[25] within semi-classical Boltzmann theory and the rigid-band approximation.[26] The thermoelectric figure of merit ZT is

$$ZT = \frac{S^2 \sigma T}{\kappa}$$

where κ is the total thermal conductivity ($\kappa = \kappa_L + \kappa_E$, with κ_L and κ_E being the lattice thermal conductivity and electronic thermal conductivity, respectively). In this work, instead of ZT, we computed the parameter $S^2\sigma$, known as the power factor.

Results and discussion

Stable Li–B compounds at ambient pressure

Stability of compounds in multicomponent systems can be evaluated from the thermodynamic convex hull construction. The calculated convex hull of the Li–B system at ambient pressure is mainly built from the results of VCS using USPEX. At a few selected chemical compositions, the structures of assumed lithium borides were also predicted using the FCS method. In addition, we also calculated the enthalpies of formation of some Li–B compounds like LiB, LiB_2, Li_3B_{14}, Na_3B_{20}-type, Na_2B_{29}-type, and NaB_{15}-type structures based on previous theoretical or experimental structural data[3–11,27–31] and compiled them in Fig. 1. In the VCS and FCS, the ambient-pressure phases of Li and B, with space groups $Im\bar{3}m$ and $R\bar{3}m$, respectively, can be reproduced readily. It can be found from Fig. 1 that besides the experimentally determined

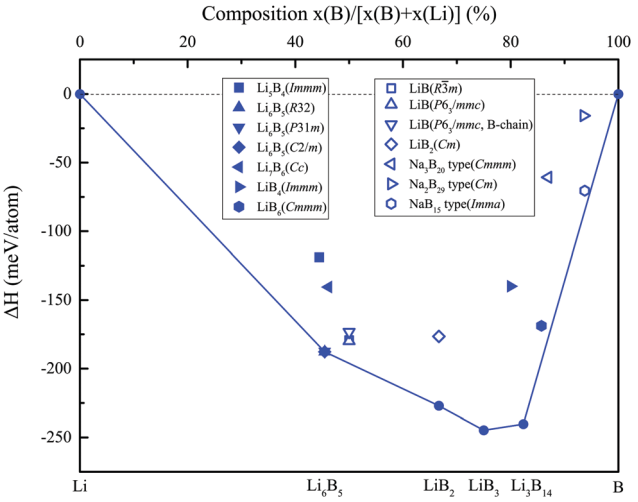

Fig. 1 Enthalpies of formation (ΔH, in meV per atom) with respect to *bcc* Li and α-B_{12} ($R\bar{3}m$) for the Li–B system at ambient pressure.

Table 1 Optimized structural parameters of Li_6B_5, LiB_2, and LiB_3 at ambient pressure

Phase	Lattice parameters (Å, deg.)	Atomic position		Coordinates x	y	z
Li_6B_5 ($R32$)	a = 4.778	Li:	3d	0.0000	0.6676	0.3324
	α = 92.2	Li:	3e	0.5000	0.8342	0.1658
		B:	1b	0.5000	0.5000	0.5000
		B:	2c	0.1000	0.1000	0.1000
		B:	2c	0.3000	0.3000	0.3000
LiB_2 ($Pnma$)	a = 6.160	Li:	4c	0.4076	0.2500	0.0511
	b = 4.452	Li:	4c	0.2080	0.7500	0.1818
	c = 7.133	B:	4c	0.2463	0.2500	0.3469
		B:	4c	0.9451	0.7500	0.8457
		B:	8d	0.6101	0.0587	0.5718
LiB_3 ($P4/mbm$)	a = 5.978	Li:	4g	0.3164	0.8164	0.0000
	c = 4.158	B:	4e	0.0000	0.0000	0.2061
		B:	8j	0.6619	0.3651	0.5000

Li_3B_{14}, three newly found phases can coexist with solid Li and B in the ground state. Their optimized lattice parameters are listed in Table 1. Especially, stoichiometric LiB based on the previous structure models is always metastable and lies above the tie line joining Li_6B_5 and LiB_2, which is consistent with the computational study by Kolmogorov and Curtarolo[32] and clearly indicates that stoichiometric LiB is less stable than nonstoichiometric LiB_x ($0.8 \leq x \leq 1$). The recent high-pressure synchrotron powder data combined with first-principles calculations also confirmed that LiB remains metastable at ambient pressure,[33] which is in agreement with our prediction. Moreover, high pressure above 20 GPa can drive the occurrence of the transition from non-stoichiometric LiB_y (down to y = 0.75) to 2D-layered stoichiometric LiB.[33] However, it must be pointed out that high-pressure stabilization of Li–B compounds is beyond the scope of current work. Crystal structures of Li_6B_5, LiB_2, and LiB_3 are shown in Fig. 2. Their detailed physical properties are discussed in the following sections. Structural data of some

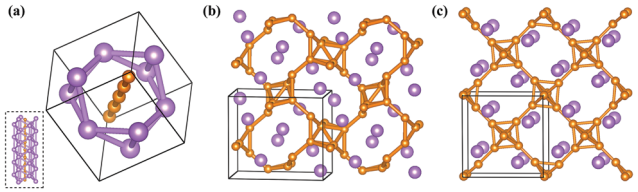

Fig. 2 Crystal structures of some stable Li–B compounds at ambient pressure: (a) Li_6B_5 (space group *R*32), (b) LiB_2 (*Pnma*), and (c) LiB_3 (*P*4/*mbm*). Large purple and small yellow spheres are Li and B, respectively. The inset in (a) presents linear chains of boron atoms surrounded by Li atoms.

low-energy metastable phases found in our simulations are listed in ESI.†

Li_6B_5: a metallic phase containing carbyne-like boron chains

Li_6B_5 found in our evolutionary structure searches has a trigonal structure with space group *R*32. In the *R*32 structure as shown in Fig. 2a, B atoms occupy the 1b and 2c atomic sites and form the linear boron chains which are encapsulated in the channels formed by Li atoms. It must be pointed out that trigonal Li_6B_5 is consistent with the structure described by Wörle and Nesper for LiB_x ($0.82 < x < 1.0$).[11] B–B, Li–B, and Li–Li distances and mass densities of Li_6B_5, along with metastable phases Li_5B_4 (*Immm*), Li_7B_6 (*Cc*), and LiB (*P*6$_3$/*mmc*) also predicted from our FCS simulations, are listed in Table 2. It can be found that the calculated values of Li_6B_5 are in good agreement with the experimental data for the nonstoichiometric LiB.[10]

Now we can give our interpretation of the initially mysterious facts – (1) non-stoichiometric formula LiB_{1-x}, and its precise composition, (2) incommensurability and (3) metallicity of this phase. The structure, when viewed along the threefold axis, can be described as consisting of straight –B–B– and –Li–Li– chains in a 1 : 2 ratio. If B–B and Li–Li distances were the same, the stoichiometry would be Li_2B. However, the sizes of Li and B are very different – their atomic radii are in a Li : B = 1.85 ratio, which would bring the "ideal" ratio of Li and B atoms to 2.0/1.85 = 1.08 (corresponding to stoichiometry $Li_{1.08}B = LiB_{0.92} = Li_{13}B_{12}$). This composition, with extra lithium atoms compared to the ideal Zintl–Klemm compound LiB, should be metallic. In metals, all ionic interactions (repulsive between Li^+ particles) are very efficiently screened, enabling Li atoms to come closer (2.649 Å in Li_6B_5, compared with 2.785 Å in LiB – see Table 2) and making the composition even more Li-rich and increasing the density of the compound. Incommensurability of the structure and disorder in the vertical position of B-chains are direct consequences of these factors and are reflected in the existence of essentially degenerate structures of Li_6B_5: $R\bar{3}$, *P*31*m*, *C*2/*m*. Our *R*32-Li_6B_5 phase is the best small-cell approximant of the real incommensurate LiB_{1-x} compound.

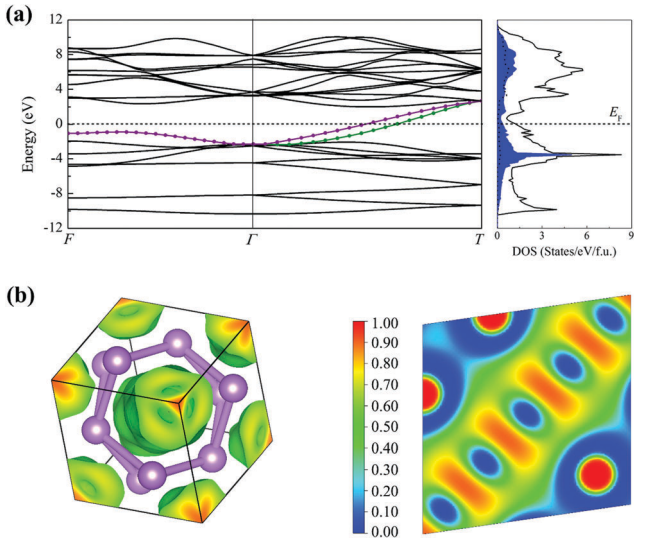

Fig. 3 Electronic structure of the *R*32 phase of Li_6B_5: (a) band structure and density of states (DOS); (b) electron localization function (ELF): ELF = 0.5 isosurface and ELF slice through the chain of boron atoms. The DOSs of B-2p and Li-2s states are depicted by a blue-shaded pattern and a dashed line, respectively.

Fig. 3 presents the calculated electronic band structure and density of states (DOS) of the *R*32 phase of Li_6B_5. Two bands marked in Fig. 3 cross the Fermi energy level (E_F), indicating metallic character of this phase. The total DOS at E_F is about 1.71 states per eV per f.u., which is mainly contributed by B-2p states. Fig. 3b shows the calculated electron localization function (ELF) of *R*32-Li_6B_5. The maximum value of ELF between B atoms is about 0.9, indicating strong covalent bonds between B atoms in the linear boron chain. At the same time, there is no ELF peak between the linear B chain and Li atoms, suggesting no covalent bonding between them.

Fig. 4 shows the calculated phonon dispersion curves, phonon DOS, and Eliashberg spectral function $\alpha^2F(\omega)$ of Li_6B_5. Two phonon bands between 15.8 and 35.7 THz can be assigned to the bending vibrations of the linear B chain. The highest-frequency bands above 35.7 THz are ascribed to the symmetric and antisymmetric stretching vibrations of B atoms. The integral of the EPC parameter $\lambda(\omega)$ is only about 0.21. Vibrations below 16.5 THz contribute about 65.9% of the total λ value. The contribution from the bending vibrations of the B chain is negligible.

Table 2 Calculated B–B, Li–Li and Li–B distances (*d*, in Å) and densities (ρ, in g cm^{-3}) for Li_6B_5 (*R*32) and metastable phases with B-chains – LiB (*P*6$_3$/*mmc*), Li_5B_4 (*Immm*), and Li_7B_6 (*Cc*) – at ambient pressure. For comparison, available experimental data for nonstoichiometric LiB are listed

	Li_6B_5	LiB	Li_5B_4	Li_7B_6	LiB (expt.)[10]
d_{B-B}	1.589–1.590	1.559	1.567–1.571	1.583–1.597	1.60
d_{Li-Li}	2.649–2.658	2.785–3.118	2.628–3.138	2.342–3.138	
d_{Li-B}	2.301–2.314	2.436	2.328–2.503	2.285–2.450	
ρ	1.46	1.37	1.25	1.43	1.43, 1.47, 1.49

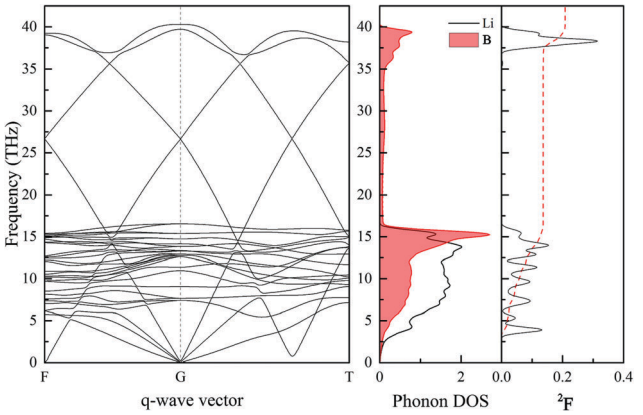

Fig. 4 Phonon dispersion curves (left), phonon density of states (PDOS) projected on Li and B atoms (middle), and Eliashberg phonon spectral function $\alpha^2F(\omega)$ together with the electron–phonon integral $\lambda(\omega)$ (right) for the *R*32 structure of Li_6B_5 at ambient pressure.

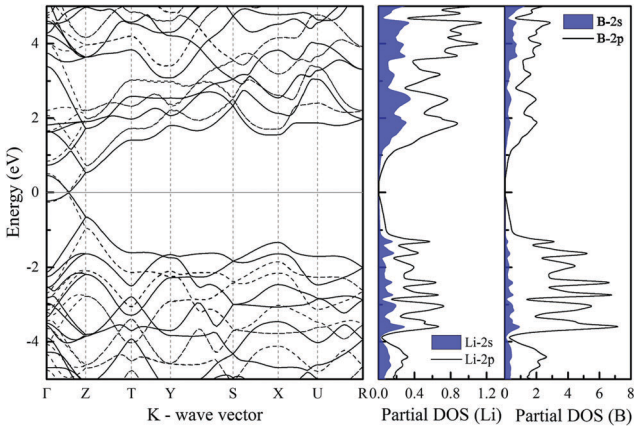

Fig. 5 Band structure of orthorhombic LiB_2 along high-symmetry directions in the Brillouin zone and partial DOS. Band structure (dashed lines) calculated within the GW quasiparticle approximation is presented for comparison.

The stretching vibrations between B atoms above 35.7 THz contribute about 34.1% of the total λ. The calculated logarithmic average frequency ω_{log} is about 325.6 K. The corresponding critical superconductivity temperature T_c, obtained from the Allen–Dynes equation using commonly accepted Coulomb pseudopotential $\mu^* = 0.10$, is only about 0.32 K. This value of T_c is somewhat lower than that of the pure metallic Li (<1.3 K).

LiB_2: a new stable phase with distinctive band structure

The crystal structure of LiB_2 predicted from our evolutionary simulations has orthorhombic symmetry with space group *Pnma*. B atoms form edge-sharing pentagonal pyramids connected into a network, and Li atoms are located in its tunnels. It must be pointed that the crystal structure of LiB_2 is very similar to that of MgB_4 which has the same symmetry (space group *Pnma*).[34] The most significant structural difference between LiB_2 and MgB_4 is that there are twice as many Li ions in the tunnels of the boron framework in LiB_2 as Mg atoms in MgB_4. This relationship is easily understood, considering their chemical formulas as $(Li^+)_2B_4$ *vs.* $(Mg^{2+})B_4$.

Fig. 5 shows the calculated band structure of *Pnma*-LiB_2. There is a crossing of valence and conduction bands at one point in the Γ–*Z* line, which is also confirmed by the GW quasiparticle calculation. The density of states at E_F is zero, and here we have a pair of touching Dirac cones, which means that *Pnma*-LiB_2 is a Dirac semimetal. A similar behavior appears in the band structure of graphene[35] and theoretically predicted 2D layered *Pmmn*-boron.[36] The 3D structure of *Pnma*-LiB_2 allows it to hold Dirac quasiparticles in the bulk and this feature can lead to many exciting physical properties, such as extraordinary transport behavior.

We further evaluated the thermoelectric properties of LiB_2 based on the semi-classical Boltzmann theory. Fig. 6a shows the carrier concentration as a function of chemical potential at 300 K. Fig. 6b shows the calculated Seebeck coefficient (S) as a function of temperature at different chemical potentials (μ). The S of undoped LiB_2 is only 56.68 μV K^{-1}, but the

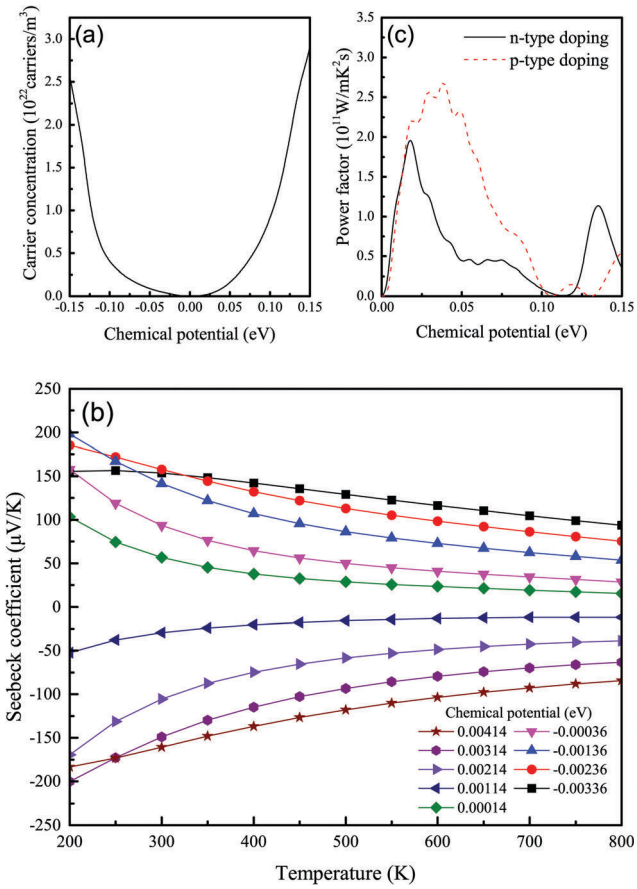

Fig. 6 Calculated thermoelectric properties of *Pnma*-LiB_2 at ambient pressure: (a) carrier concentration as a function of chemical potential at 300 K; (b) Seebeck coefficient *versus* temperature at various chemical potentials; (c) relationship of power factor ($S^2\sigma/\tau$) with carrier concentration at 300 K.

thermoelectric properties change with the doping level. For n-type doping, the thermopower increases dramatically as the chemical potential of the electron increases, and can reach

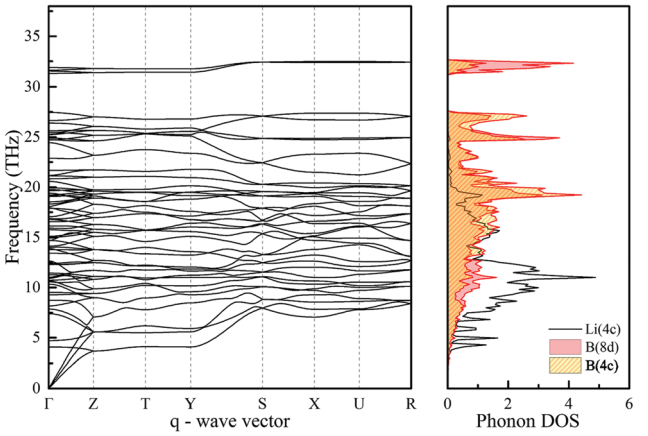

Fig. 7 Phonon dispersion curves and phonon density of states (PDOS) projected on Li and B atoms for the *Pnma* structure of LiB_2 at ambient pressure.

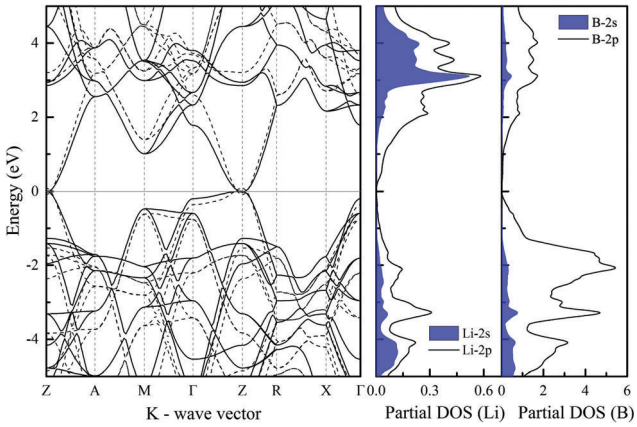

Fig. 8 Band structure of tetragonal LiB_3 along high-symmetry directions in the Brillouin zone, and partial DOS. Band structure (dashed lines) calculated within the GW quasiparticle approximation is presented for comparison.

-160.72 μV K^{-1} at $\mu = 0.004$ eV at 300 K. For p-type doping, the thermopower increases to about 157.85 μV K^{-1} at $\mu = -0.002$ eV at 300 K. The calculated power factor $S^2\sigma/\tau$ of LiB_2 is depicted in Fig. 6c. Both n-type and p-type doping can increase the power factor. For p-type doping, the maximum value of $S^2\sigma/\tau$ is 2.68×10^{11} W m^{-1} K^{-2} s^{-1} which occurs at $\mu = 0.038$ eV, and for n-type doping the maximum value of the power factor is 1.94×10^{11} W m^{-1} K^{-2} s^{-1} at $\mu = -0.019$ eV.

Fig. 7 shows the calculated phonon dispersion curves along the high-symmetry directions in the Brillouin zone and projected phonon DOS for *Pnma*-LiB_2. Low-frequency vibrations below 20 THz mainly come from Li atoms, but coupled Li–B translational motions are also not negligible. In the higher-frequency region between 20 and 28 THz, the phonon spectrum is mainly due to the librational motions of B atoms. The flat bands at around 32 THz can be assigned to the stretching vibrations of B atoms.

LiB_3: a semimetal with a high thermoelectric power factor

LiB_3 found in our simulations has a tetragonal structure with space group *P*4/*mbm*. As shown in Fig. 2c, B atoms form B_6-octahedra linked into a network, with Li atoms occupying the channels in it. In fact, this structure is identical to the crystal structure of LiB_3 reported by Nesper.[5]

Fig. 8 presents the calculated electronic band structure and DOS of the *P*4/*mbm* phase of LiB_3. Like LiB_2, it is a zero-gap semimetal. The valence and conduction bands touch at the *Z* point and form massive (*e.g.* non-massless) Dirac cones. The bands near E_F are more dispersive than in LiB_2, which results in a smaller carrier concentration, disadvantageous for thermoelectric properties. However, there is a section of flat valence bands along the *Γ*–*Z* path very close to the Fermi level. This may be favorable for thermopower after doping.

From Fig. 9a, we can see that for increasing carrier concentration, n-type doping is more efficient than p-type doping for LiB_3, because of the flat band along the *Γ*–*Z* direction in LiB_3. The calculated *S* as a function of temperature at different chemical potentials depicted in Fig. 9b shows that pure LiB_3 has a negligible thermopower and is insensitive to the change of temperature.

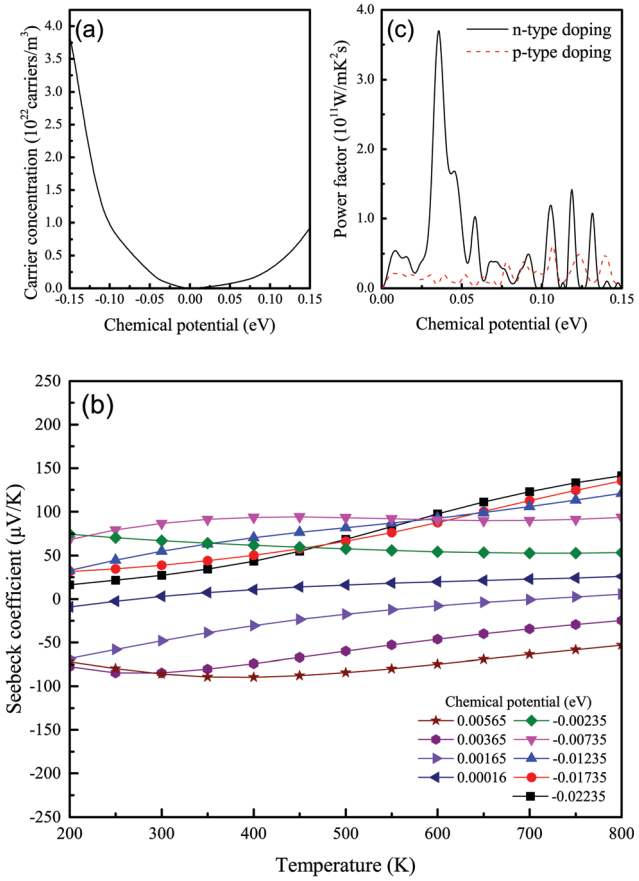

Fig. 9 Calculated thermoelectric properties of *P*4/*mbm*-LiB_3 at ambient pressure: (a) carrier concentration as a function of chemical potential at 300 K; (b) Seebeck coefficient *versus* temperature at various chemical potentials; (c) relationship of power factor ($S^2\sigma/\tau$) with carrier concentration at 300 K.

Under room temperature, the p-type doping can increase the thermopower up to -89.21 μV K^{-1} at $\mu = 0.006$ eV. Especially, minor n-type doping has a good effect on the thermopower.

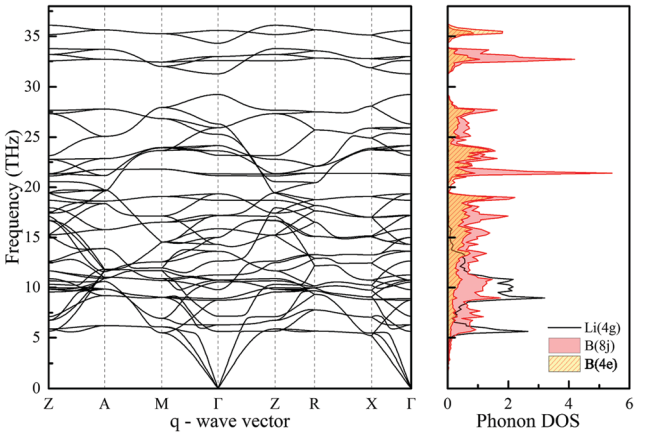

Fig. 10 Phonon dispersion curves and phonon density of states (PDOS) projected on Li and B atoms for the *P*4/*mbm* structure of LiB_3 at ambient pressure.

At room temperature, the maximum value of S is 86.86 μV K^{-1} at $\mu = -0.007$ eV, but when the chemical potential μ is increased a little further, S starts to go up with increasing temperature. The value of S reaches 141.37 μV K^{-1} at 800 K when $\mu = -0.022$ eV. As shown in Fig. 9c, the change in the power factor $S^2\sigma/\tau$ with the chemical potential of LiB_3 is obviously different from that of LiB_2 (see Fig. 6c). The value of $S^2\sigma/\tau$ reaches 3.69×10^{11} W m^{-1} K^{-2} s^{-1} when μ is −0.035 eV for n-type doping, which is 7 times higher than the maximum value for p-type doping (0.51×10^{11} W m^{-1} K^{-2} s^{-1}) at $\mu = 0.109$ eV. The traditional thermoelectric material Bi_2Te_3 has an obviously larger maximum S of 300 μV K^{-1}, and it also has larger $S^2\sigma/\tau$ of 1.2×10^{12} W m^{-1} K^{-2} s^{-1}.[37] However, the calculated power factor of LiB_3 is comparable to the value of another environment-friendly thermoelectric material, Sn doped Mg_2Si (0.87×10^{11}–5.2×10^{11} W m^{-1} K^{-2} s^{-1}).[38] As a result, although LiB_3 has a smaller S than LiB_2, the higher value of $S^2\sigma/\tau$ resulting from minor n-type doping makes LiB_3 a more promising thermoelectric material than LiB_2.

Fig. 10 shows the calculated phonon dispersion curves and phonon density of states. Contribution of Li atoms is particularly prominent at low frequencies (<13 THz), and one can note different frequency ranges of B(4e) and B(8j) atoms, or more precisely, their different relative contributions at different frequencies.

Conclusion

From the global *ab initio* evolutionary search for stable compounds and crystal structures, we built the complete thermodynamic convex hull for the Li–B binary system at ambient pressure, and determined the crystal structures of stable Li–B compounds including Li_6B_5, LiB_2, and LiB_3. Li_6B_5, the first structure found in our work has space group *R*32, and this metallic phase contains the characteristic linear B chains surrounded by Li atoms. Our electron–phonon coupling calculations indicate that Li_6B_5 cannot be a good superconductor. The predicted orthorhombic LiB_2 (*Pnma*) and tetragonal LiB_3 (*P*4/*mbm*) are semimetals, with promising thermoelectric properties (especially LiB_3). In addition, LiB_2 is a 3D-solid with massless Dirac fermions.

Acknowledgements

This work was supported by the National Basic Research Program of China (Grant No. 2014CB643703), the National Natural Science Foundation of China (Grant No. 11464008 and 51401060), the Guangxi Natural Science Foundation (Grant No. 2014GXNSFGA118001 and 2016GXNSFGA380001), the Fund from Guangxi Key Laboratory of Information Materials (Grant No. 1210908-215-Z and 131022-Z), and the Research Foundation of Guangxi Experiment Center of Information Science (Grant No. YB1512). ARO acknowledges support from DARPA (Grant No. W31P4Q1210008) and Foreign Talents Introduction and Academic Exchange Program (No. B08040).

References

1 N. N. Greenwood and A. Earnshaw, *Chemistry of the Elements*, Pergamon Press, New York, 1984.
2 B. Albert and H. Hillebrecht, Boron: Elementary Challenge for Experimenters and Theoreticians, *Angew. Chem.*, 2009, **48**(46), 8640–8668.
3 J. Nagamatsu, N. Nakagawa, T. Muranaka, Y. Zenitani and J. Akimitsu, Superconductivity at 39 K in Magnesium Diboride, *Nature*, 2001, **410**(6824), 63–64.
4 G. Mair, R. Nesper and H. G. von Schnering, Trilithium Tetradecaboride Li_3B_{14}: Synthesis, Structure, and Properties, *J. Solid State Chem.*, 1988, **75**(1), 30–40.
5 G. Mair, H. G. von Schnering, M. Wörle and R. Nesper, Dilithium hexaboride, Li_2B_6, *Z. Anorg. Allg. Chem.*, 1999, **625**(7), 1207–1211.
6 F. E. Wang, M. A. Mitchell, R. A. Sutula, J. R. Holden and L. H. Bennett, Crystal Structure Study of a New Compound Li_5B_4, *J. Less-Common Met.*, 1978, **61**(2), 237–251.
7 F. E. Wang, An Unusual Phenomenon in the Formation of Li_5B_4 Compound-alloy, *Metall. Trans. A*, 1979, **10**(3), 343–348.
8 P. Sanchez, C. Belin, G. Crepy and A. De Guibert, Preparation and Characterization of Lithium-Boron Alloys: Electrochemical Studies as Anodes in Molten Salt Media, and Comparison with Pure Lithium-involving Systems, *J. Mater. Sci.*, 1992, **27**(1), 240–246.
9 S. Dallek, D. W. Ernst and B. F. Larrick, Thermal Analysis of Lithium-Boron Alloys, *J. Electrochem. Soc.*, 1979, **126**(5), 866–870.
10 Z. Liu, X. Qu, B. Huang and Z. Li, Crystal Structure and Morphology of a New Compound, LiB, *J. Alloys Compd.*, 2000, **311**(2), 256–264.
11 H. Rosner and W. E. Pickett, Theoretical Investigation of Stoichiometric Lithium Monoboride, *Phys. Rev. B: Condens. Matter Mater. Phys.*, 2003, **67**(5), 054104.

12 M. Wörle and R. Nesper, Infinite, Linear, Unbranched Borynide Chains in LiB_x—Isoelectronic to Polyyne and Polycumulene, *Angew. Chem., Int. Ed.*, 2000, **39**(13), 2349–2353.
13 A. R. Oganov and C. W. Glass, Crystal Structure Prediction Using Ab-initio Evolutionary Techniques: Principles and Applications, *J. Chem. Phys.*, 2006, **124**(24), 244704.
14 A. O. Lyakhov, A. R. Oganov, H. T. Stokes and Q. Zhu, New Developments in Evolutionary Structure Prediction Algorithm USPEX, *Comput. Phys. Commun.*, 2013, **184**(4), 1172–1182.
15 A. R. Oganov, J. Chen, C. Gatti, Y. Ma, Y. Ma, C. W. Glass, Z. Liu, T. Yu, O. O. Kurakevych and V. L. Solozhenko, Ionic High-pressure Form of Elemental Boron, *Nature*, 2009, **457**(7231), 863–867.
16 G. Saleh and A. R. Oganov, Alkali subhalides: high-pressure stability and interplay between metallic and ionic bonds, *Phys. Chem. Chem. Phys.*, 2016, **18**, 2840.
17 A. O. Lyakhov, A. R. Oganov and M. Valle, Crystal Structure prediction using evolutionary approach, in *Modern methods of crystal structure prediction*, ed. A. R. Oganov, Berlin, Wiley-VCH, 2010, pp. 147–180.
18 A. R. Oganov, Y. Ma, A. O. Lyakhov, M. Valle and C. Gatti, Evolutionary crystal structure prediction as a method, for the discovery of minerals and materials, *Rev. Mineral. Geochem.*, 2010, **71**, 271–298.
19 G. Kresse and J. Furthmüller, Efficient Iiterative Schemes for Ab-initio Total-energy Calculations Using a Plane-wave Basis Set, *Phys. Rev. B: Condens. Matter Mater. Phys.*, 1996, **54**(16), 11169–11186.
20 P. E. Blochl, Projector Augmented-wave Method, *Phys. Rev. B: Condens. Matter Mater. Phys.*, 1994, **50**(24), 17953–17979.
21 J. P. Perdew, K. Burke and M. Ernzerhof, Generalized Gradient Approximation Made Simple, *Phys. Rev. Lett.*, 1996, **77**(18), 3865–3868.
22 M. Shishkin and G. Kresse, Implementation and Performance of the Frequency-dependent GW Method within the PAW Framework, *Phys. Rev. B: Condens. Matter Mater. Phys.*, 2006, **74**(3), 035101.
23 A. Togo and I. Tanaka, First Principles Phonon Calculations in Materials Science, *Scr. Mater.*, 2015, **108**, 1–5.
24 G. Paolo, B. Stefano, B. Nicola, C. Matteo, C. Roberto, C. Carlo, C. Davide, L. C. Guido, C. Matteo, D. Ismaila, C. Andrea Dal, G. Stefano de, F. Stefano, F. Guido, G. Ralph, G. Uwe, G. Christos, K. Anton, L. Michele, M.-S. Layla, M. Nicola, M. Francesco, M. Riccardo, P. Stefano, P. Alfredo, P. Lorenzo, S. Carlo, S. Sandro, S. Gabriele, P. S. Ari, S. Alexander, U. Paolo and M. W. Renata, QUANTUM ESPRESSO: A Modular and Open-source Software Project for Quantum Simulations of Materials, *J. Phys.: Condens. Matter*, 2009, **21**(39), 395502.
25 G. K. H. Madsen and D. J. Singh, BoltzTraP. A Code for Calculating Band-structure Dependent Quantities, *Comput. Phys. Commun.*, 2006, **175**(1), 67–71.
26 T. J. Scheidemantel, C. Ambrosch-Draxl, T. Thonhauser, J. V. Badding and J. O. Sofo, Transport Coefficients from First-principles Calculations, *Phys. Rev. B: Condens. Matter Mater. Phys.*, 2003, **68**(12), 125210.
27 P. Hagenmuller and R. Naslain, L'hexaboruce NaB_6, *Comptes Rendus de l'Académie des Sciences*, 1963, **257**, 1294–1296.
28 R. Naslain and J. S. Kasper, The Crystal Structure of the Φ Phase in the Boron-sodium System, *J. Solid State Chem.*, 1970, **1**(2), 150–151.
29 R. Naslain, A. Guette and P. Hagenmuller, Crystal Chemistry of Some n-rich Phases, *J. Less-Common Met.*, 1976, **47**, 1–16.
30 A. Hermann, A. McSorley, N. W. Ashcroft and R. Hoffmann, From Wade–Mingos to Zintl–Klemm at 100 GPa: Binary Compounds of Boron and Lithium, *J. Am. Chem. Soc.*, 2012, **134**(45), 18606–18618.
31 F. Peng, M. Miao, H. Wang, Q. Li and Y. Ma, Predicted Lithium–Boron Compounds Under High Pressure, *J. Am. Chem. Soc.*, 2012, **134**(45), 18599–18605.
32 A. N. Kolmogorov and S. Curtarolo, Prediction of Different Crystal Structure Phases in Metal Borides: A Lithium Monoboride Analog to MgB_2, *Phys. Rev. B: Condens. Matter Mater. Phys.*, 2006, **73**(18), 180501.
33 A. N. Kolmogorov, S. Hajinazar, C. Angyal, V. L. Kuznetsov and A. P. Jephcoat, Synthesis of a predicted layered LiB *via* cold compression, *Phys. Rev. B: Condens. Matter Mater. Phys.*, 2015, **92**, 144110.
34 M. M. Roger Naslain, A. Guette and M. Barret, Sur le Diborure et le Tétraborure de Magnésium. Considérations Cristallochimiques sur les Tétraborures, *J. Solid State Chem.*, 1973, **8**(1), 68–85.
35 K. S. Novoselov, A. K. Geim, S. V. Morozov, D. Jiang, M. I. Katsnelson, I. V. Grigorieva, S. V. Dubonos and A. A. Firsov, Two-dimensional gas of massless Dirac fermions in graphene, *Nature*, 2005, **438**, 197.
36 X.-F. Zhou, X. Dong, A. R. Oganov, Q. Zhu, Y.-J. Tian and H.-T. Wang, Semimetallic Two-dimensional Boron Allotrope with Massless Dirac Fermions, *Phys. Rev. Lett.*, 2014, **112**, 085502.
37 T. J. Scheidemantel, C. Ambrosch-Draxl, T. Thonhauser, J. V. Badding and J. O. Sofo, Transport coefficients from first-principles calculations, *Phys. Rev. B: Condens. Matter Mater. Phys.*, 2003, **68**, 125210.
38 X. J. Tan, W. Liu, H. J. Liu, J. Shi, X. F. Tang and C. Uher, Multiscale calculations of thermoelectric properties of n-type $Mg_2Si_{1-x}Sn_x$ solid solutions, *Phys. Rev. B: Condens. Matter Mater. Phys.*, 2012, **85**, 205212.